PAPER

Dependence of Thermal Annealing on Transparent Conducting Properties of HoF_3-Doped ZnO Thin Films*

CHIN. PHYS. LETT. Vol. 36, No. 5 (2019) 057303

Dependence of Thermal Annealing on Transparent Conducting Properties of HoF_3-Doped ZnO Thin Films *

Jin-Song Luo(罗劲松)[1,2], Jie Lin(林杰)[2**], Li-Gong Zhang(张立功)[2], Xiao-Yang Guo(郭晓阳)[2], Yong-Fu Zhu(朱永福)[1**]

[1]*Key Laboratory of Automobile Materials, Ministry of Education, and School of Materials Science and Engineering, Jilin University, Changchun 130022*

[2]*State Key Laboratory of Luminescence and Applications, Changchun Institute of Optics, Fine Mechanics and Physics, Chinese Academy of Sciences, Changchun 130033*

(Received 19 February 2019)

A kind of n-type HoF_3-doped zinc oxide-based transparent conductive film has been developed by electron beam evaporation and studied under thermal annealing in air and vacuum at temperatures 100–500°C. Effective substitutional dopings of F to O and Ho to Zn are realized for the films with smooth surface morphology and average grain size of about 50 nm. The hall mobility, electron concentration, resistivity and work function for the as-deposited films are 47.89 cm^2/Vs, 1.39×10^{20} cm^{-3}, 9.37×10^{-4} Ω·cm and 5.069 eV, respectively. In addition, the average transmittance in the visible region (400–700 nm) approximates to 87%. The HoF_3:ZnO films annealed in air and vacuum can retain good optoelectronic properties under 300°C, thereinto, more stable electrical properties can be found in the air-annealed films than in the vacuum-annealed films, which is assumed to be a result of improved nano-crystalline lattice quality. The optimized films for most parameters can be obtained at 200°C for the air-annealing case and at room temperature for the vacuum annealing case. The advisable optoelectronic properties imply that HoF_3:ZnO can facilitate carrier injection and has promising applications in energy and light sources as transparent electrodes.

PACS: 73.90.+f, 78.90.+t, 78.66.Hf, 81.15.Ef

DOI: 10.1088/0256-307X/36/5/057303

Transparent conductive oxide (TCO) films has been a hot topic in optoelectronic fields.[1–3] Indium tin oxide (ITO), as a typical application case, has been widely used as transparent electrodes in liquid crystal displays, solar cells and light-emitting diodes because of high conductive and transparent properties, good stability and mature technology.[4–5] However, expensive raw materials and less resource on earth limit its future usage.

Doped ZnO films, such as Al-doped ZnO (AZO), In-doped ZnO and Ga-doped ZnO, are currently under intense investigation due to advantages including cheap and abundant raw materials, ultraviolet absorption tailoring, high stability in a hydrogen plasma and easy manufacturing.[6–8] Among them, AZO films take the lead in commercialization. In addition to single-element doping, dual-element co-doping technologies, such as F/Al, F/Ga, F/Sn, and F/Eu, have been employed to further raise optoelectronic properties of ZnO films.[9–12] Annealing treatment is another effective technology to optimize overall performance of materials. However, annealing treatment for ZnO-based films is mainly under vacuum or inert atmosphere, which is rare in air and not conducive to ambient industrial processing at high temperature. In this work, we have developed a new HoF_3-doped ZnO film based on our previous study.[12] The main focus is on comparison of thermal stability in air and vacuum in order to provide a reference for practical application of HoF_3-doped ZnO films.

The HoF_3-doped ZnO films were deposited on glass or silicon substrates by electron beam (e-beam) evaporation with end-Hall ion assisted deposited (IAD) technology. HoF_3 and ZnO powders (ZnO 99% purity, HoF_3 99% purity, and the ratio of Ho:Zn = 3.5 at%) were blended and milled by using planet type ball mill for 20 h, then were pressed to compact, held in a copper crucible. The deposition rate and thickness were monitored in situ by a thin film deposition controller (MDC-360 C), which were 2.3–2.7 Å/s and 150 nm, respectively. The evaporation chamber was initially evacuated at a base pressure of 1.0×10^{-3} Pa, and then argon gas was introduced into the end-Hall ion source and evaporation chamber at the optimized flow rate of 1.0 and 8.0 sccm, respectively. The operating pressure was 3.4×10^{-2} Pa. The substrate temperature was controlled at 300℃ during deposition. After deposition, the samples were annealed at different temperatures. The heating temperature was from 100℃ to 500℃ at a rate of 4℃/min in air and 100 Pa vacuum, and kept 60 min in vacuum tube furnace (SGL-100, China). After annealing, the samples were cooled naturally to room temperature (RT).

Carrier concentration, resistivity, and mobility were measured by an HMS-3000 Hall effect measurement system. Optical transmittance spectra were measured with a Shimadzu UV-3101 PC spectropho-

*Supported by the National Natural Science Foundation of China under Grant Nos 61774154 and 51503196.

**Corresponding author. Email: linj@ciomp.ac.cn; yfzhu@jlu.edu.cn

tometer. The crystallographic structure was analyzed by x-ray diffraction (XRD). The film thickness was calibrated by a surface profiler (Alpha-step 500). Surface morphology was observed by a field emission scanning electron microscope (FESEM, XL-40). The work function was investigated by a KP Technology Ambient Kelvin probe system package.

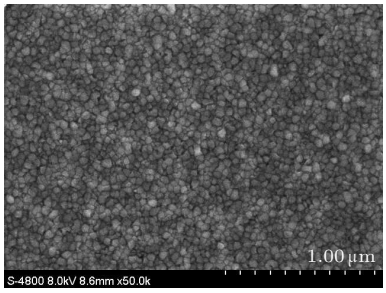

Fig. 1. SEM image of the as-deposited film.

Because it is difficult to identify obvious difference between the morphologies of the samples with and without annealing, only the typical sample morphology without annealing is given. The SEM image in Fig. 1 illustrates that the as-deposited (unannealed) film is composed of nano particles with the average grain size of about 50 nm. The closely stacked nano particles form a smooth film without holes or cracks. Energy dispersive spectra (EDS) give obvious signal of Ho and F atoms. However, the quantitative content of HoF_3 in ZnO estimated by the EDS is close to 1.7 at% and much less than the doping concentration of 3.5 at% in the raw materials. This can be attributed to the difference of vapor pressure for HoF_3 and ZnO in the e-beam deposition process.

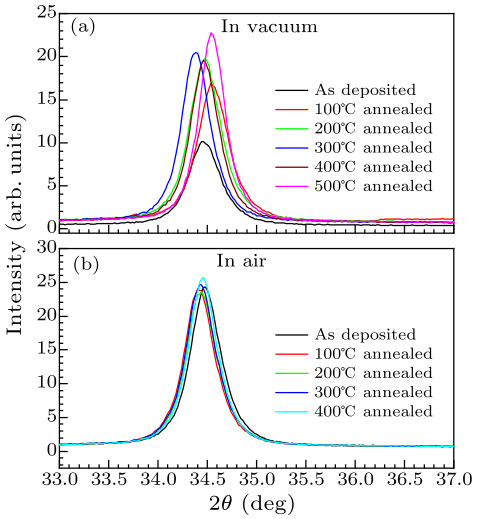

Fig. 2. XRD pattern of the as-deposited and annealed HoF_3-doped ZnO thin films at different temperatures: (a) in vacuum, (b) in air.

Figure 2 shows that the as-deposited film exhibits a dominant diffractive peak of (002) ZnO crystal plane at 34.44°. There are no other characteristic peaks of Ho/F ions appearing in the pattern, indicating an effective incorporation of F/Ho into ZnO lattice. As ion radius difference is −5.6% between F^- (1.17 Å) and O^{2-} (1.24 Å), and +21.7% between Ho^{3+} (0.901 Å) and Zn^{2+} (0.74 Å),[13] the complementary ion radius difference would facilitate substitutional doping. Simultaneously, doped F^- ions could passivate oxygen vacancy defect,[14] so free carriers come mainly from Ho/F shallow donor impurities.

The vacuum annealing leads to a fluctuation in the 34.44° diffraction peak, which can be attributed to the deformation of crystal lattice induced by the spread of defection or doping atoms. Diffraction peaks show a negligible deviation below 100℃ and a shift to a lower angle at 100–300℃, indicating occurrence of lattice dilatation. However, further improvement of annealing temperature will cause larger-angle-shifted diffraction peaks and thus a lattice shrinkage. Synthetic effect of diffusion of defects and doping atoms, grain boundary, chemical adsorption and desorption of some elements, and re-evaporation of high vapor pressure atoms could be the possible reasons. Compared to the vacuum annealing case, diffraction peak fluctuation under air annealing is little, which implies that the oxygen vacancy defect concentration is in a negligible level. The full width at half maximum (FWHM) of the (002) diffraction peak shows a slight and monotonous drop with the increasing temperature in vacuum and air, indicating an improved crystallization of the samples.

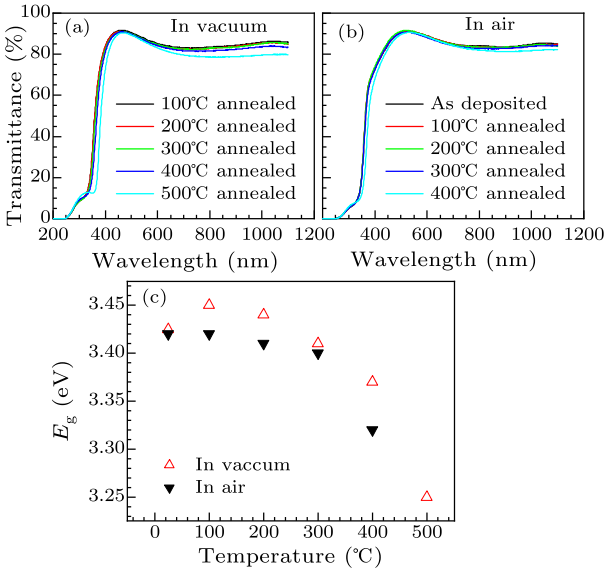

Fig. 3. Transmittance spectra of the as-deposited and annealed HoF_3-doped ZnO thin films at different temperatures in vacuum (a) and in air (b). (c) The calculated band-gap energy.

Figures 3(a) and 3(b) show the optical transmission spectra of the samples. The average transmittance T_{ave} of the as-deposited samples is about 87% in the visible region (400–700 nm). There reveals an absorption-edge at the short wave side of 400 nm due

to the intrinsic band-gap transition of ZnO films. For the vacuum annealing case, the 100℃-annealed samples have a maximum transmittance T_{max} of 91.7% at 459 nm and T_{ave} of 87.2%. Both T_{max} and T_{ave} exhibit the similar monotonous decrease with the temperature increasing in the range 100–500℃, which can be attributed to the slightly raised refractive index due to the increased packing density or crystallization of the samples. When annealed at 500℃, the T_{max} and T_{ave} drop to 90.4% and 84.7%, respectively. For the air annealing case, T_{max} and T_{ave} decrease first, then increase below 200℃, and then monotonously decrease with the temperature increasing in the range 200–400℃. Therefore, the 200℃-annealed samples have the highest T_{max} of 91.6% and T_{ave} of 87.3%. From RT to 400℃ without consideration of 200℃, the variation range is 85.8–86.9% for T_{ave}, and 90.7–91.3% for T_{max}. The maximum and minimum transmittance wavelength is caused by optical interference effect and shows a little variation under annealing due to the change of refractive index. The changes of optical properties for vacuum and air-annealed samples are quite similar under 300℃.

The band-gap energy E_g of the HoF_3-doped ZnO films can be estimated from the band edge absorption in optical spectra. Based on the direct-band transition, we extract the band-gap energy using the relation

$$\alpha h\nu = B\left(h\nu - E_g\right)^{1/2}, \tag{1}$$

where $h\nu$ is the photon energy, α is the absorption coefficient, and B is a constant. The extracted E_g is plotted in Fig. 3(c). For the vacuum thermal annealing, E_g rises with temperature up to 100℃, then decreases slowly with the increasing temperature, and rebounds nearly to the as-deposited one at 300℃. The observed E_g broadening below 200℃ is consistent to the Burstein–Moss effect, suggesting a rising electron density. The band-gap narrowing under higher vacuum annealing temperature implies that diffusion of defects and doping atoms, and re-evaporation may lower the substitutional doping effect. Thermal annealing in air induces a 0.02 eV small drop in E_g under 300℃ annealing. An obvious drop occurs when further lifting annealing temperature. This monotonous decline indicates the existence of other effects in the air-annealing case, whose electronic state is more stable than the vacuum-annealing case under 300℃ as a result of many factors acting together.

Generally, optical transmittance would show evidently declining with the increase of carrier density, and little drop with the increase of mobility. The as-deposited samples have sheet resistance of around 65 Ω/sq and electrical resistivity of 9.37×10^{-4} Ω·cm, respectively. In addition, the hall effect measurement demonstrates that mobility and electron concentration are about 47.89 cm^2/Vs and 1.39×10^{20} cm^{-3}, respectively. The work-function value is around 5.069 eV.

Resistivity is determined by carrier mobility and concentration. The lattice deformation and interface of crystal grains could affect the carrier mobility strongly. Figures 4(a) and 4(b) show that after annealing in vacuum and air, the resistivity and mobility increase monotonously and decrease monotonously, respectively. Therefore, compared with the annealed samples, the as-deposited samples have the minimum resistivity and maximum mobility. Compared with the as-deposited case, under 300℃, the resistivity increases 15% for the air-annealed ones and 53% for the vacuum-annealed ones. The mobility decreases 29% for the vacuum-annealed samples and 17% for the air-annealed ones. The resistivity of the air and vacuum 400℃-annealed samples increases 21 times and 3.2 times, respectively, and the mobility decreases 92% and 62%, respectively.

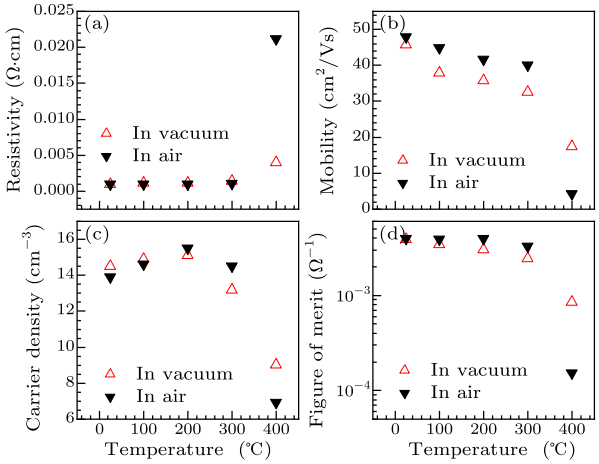

Fig. 4. Dependence of (a) resistivity, (b) mobility, (c) carrier density, and (d) figure of merit for HoF_3-doped ZnO films on annealing temperature in air and vacuum.

In general, thermal effect on resistivity under high temperature reflects the deformation in nanocrystalline lattice and the changes in defect states, which ionize or capture the carriers. The increase of resistivity is mainly caused by the decrease of mobility. Under vacuum annealing, the main factors affecting mobility are the concentration of vacancy defects, the diffusion of doped atoms and defects, grain boundaries, chemical desorption of some elements, and the re-evaporation of high vapor pressure atoms. The main factors under air-annealing are the diffusion of doped atoms and defects, chemical adsorption of some elements, and grain boundaries. The effect of vacancy defect concentration can be negligible. Therefore, the major deterioration of resistivity for the air 400℃-annealed samples may be due to chemical adsorption and desorption of some elements, and the other comprehensive factors mentioned above, as well as the effect of deep level defects on carrier concentration.

Figure 4(c) shows that below 200℃, compared with the as-deposited case, the electron densities under the air and vacuum annealing increases 11% and

4%, respectively, with the rising of annealing temperature. The electron density decreases when further improves annealing temperature to 400℃, which decreases 51% and 38%, respectively, in the air and vacuum annealing cases compared with the as-deposited one. This implies that high temperature can bring deep level defects to capture the carriers. The electron density and mobility annealed in air have smaller variations than those in vacuum below 300℃. The optimum electron density is $1.55 \times 10^{20}\,\mathrm{cm}^{-3}$ for air annealing, and $1.51 \times 10^{20}\,\mathrm{cm}^{-3}$ for vacuum annealing, both at 200℃.

The quality of TCO films can be assessed by a figure of merit calculated using the following Haacke equation.

$$\varphi_{\mathrm{TC}} = \frac{T^{10}}{Rs}, \tag{2}$$

where T is the transmittance and Rs is the sheet resistance. Here the average transmittance (400–700 nm) is chose to T, and Rs at different annealing temperatures is obtained from the resistivity divided by film thickness. Figure 4(d) demonstrates that under vacuum annealing, the φ_{TC} decreases monotonously with temperature, and the maximum φ_{TC} of the as-deposited samples is $0.00388\,\Omega^{-1}$. Under air annealing, the φ_{TC} decreases first, then increases below 200℃, after that, it decreases monotonously at 200–400℃. Therefore, the optimized φ_{TC} is $0.00397\,\Omega^{-1}$ at 200℃. The φ_{TC} annealed in air is basically better than that in vacuum below 300℃. The φ_{TC} values for air and vacuum annealing cases decrease 96% and 78%, respectively, at 400℃ in comparison to that for the as-deposited one.

In conclusion, we have developed a kind of HoF_3-doped ZnO thin films by electron beam evaporation. The x-ray diffraction spectra show that dual-element co-doping does not change the original structure of ZnO, and the as-deposited films are polycrystalline with the hexagonal structure and present a (002) preferential growth. The good conductivity and transparent properties suggest that Ho^{3+} and F^- can act as effective shallow donor impurities for wide-band gap ZnO films. Optoelectronic properties of the samples can be optimized by thermal annealing on account of the reconstruction of microstructure and change of crystal lattice quality. With the increase of annealing temperature, for the vacuum annealing case, the $T_{\max}$ and T_{ave}, mobility and φ_{TC} decrease monotonously, while the resistivity increases monotonously, for the air annealing case, mobility decreases monotonously and the resistivity increases monotonously. The $T_{\max}$, T_{ave} and φ_{TC} decrease first, then increase below 200℃, after that, monotonously decrease in the range 200–400℃. For the above-mentioned two annealing cases, the electron concentration increases first below 200℃, then decreases at 200–400℃. For the vacuum-annealing case, the as-deposited samples have the optimum values of 91.7% for $T_{\max}$, 87.2% for T_{ave}, $9.43\times10^{-4}\,\Omega\cdot$cm for resistivity, $45.8\,\mathrm{cm}^2/\mathrm{Vs}$ for mobility, and $0.00388\,\Omega^{-1}$ for φ_{TC}, respectively. In addition, the optimal electron concentration is $1.55 \times 10^{20}\,\mathrm{cm}^{-3}$ at 200℃-annealing. For the air-annealed case, the as-deposited samples have the optimum values of $9.37\times10^{-4}\,\Omega\cdot$cm for resistivity, and $47.9\,\mathrm{cm}^2/\mathrm{Vs}$ for mobility. Under 200℃-annealing, the samples have the optimal values, which are 91.6% for $T_{\max}$, 87.3% for T_{ave}, $1.51 \times 10^{20}\,\mathrm{cm}^{-3}$ for electron concentration, and $0.00397\,\Omega^{-1}$ for φ_{TC}. Under 300℃, the air-annealed samples have more stable electrical properties and better quality factors than those annealed in vacuum, and the changes in optical properties are comparable. From the view of application, HoF_3-doped ZnO thin films can be used as transparent electrodes in solar energy, display and lighting devices.

References

[1] Ephraim J, Lanigan D, Staller C, Milliron D J and Thimsen E 2016 *Chem. Mater.* **28** 5549
[2] Guo X, Liu Q L, Tian H J, Guo C W, Li C, Hu A Q, He X Y and Wu H 2018 *Chin. Phys. B* **27** 098502
[3] Xu Y, Zhang Y T, Kou Z Q, Cheng S and Bu S L 2016 *Chin. Phys. Lett.* **33** 048501
[4] Solodar A, Cerkauskaite A, Drevinskas R, Kazansky P G and Abdulhalim I 2018 *Appl. Phys. Lett.* **113** 081603
[5] Khurram A A, Imran M, Khan N A and Mehmood M N 2017 *J. Semicond.* **38** 093001
[6] Qin G P, Zhang H, Ruan H B, Wang J, Wang D and Kong C Y 2019 *Chin. Phys. Lett.* **36** 047301
[7] Sarma B, Barman D and Sarma B K 2019 *Appl. Surf. Sci.* **479** 786
[8] Lee S, Cheon D, Kim W J, Ahn K J and Lee W 2011 *Semicond. Sci. Technol.* **26** 115007
[9] Kim I, Lee K S, Lee T S, Jeong J H, Cheong B K, Baik Y J and Kim W M 2006 *J. Appl. Phys.* **100** 063701
[10] Shi Q, Zhou K, Dai M, Lin S, Hou H, Wei C and Hu F 2014 *Ceram. Int.* **40** 211
[11] Mallick A, Sarkar S, Ghosh T and Basak D 2015 *J. Alloys Compd.* **646** 56
[12] Luo J S, Lin J, Zhang N, Guo X Y, Zhang L G, Hu Y S, Lv Y, Zhu Y F and Liu X Y 2018 *J. Mater. Chem. C* **6** 5542
[13] Shannon R D 1976 *Acta Crystallogr. Sect. A* **32** 751
[14] Choi Y J, Kang K M and Park H H 2015 *Sol. Energ. Mater. Sol. C* **132** 403